NASA TECHNICAL NOTE

NASA TN D-4989

NASA TN D-4989

TRANSPORT STUDY OF NEUTRON AND PHOTON ATTENUATION THROUGH LITHIUM HYDRIDE AND TUNGSTEN SPHERICAL MEDIA

by John A. Peoples and Daniel Fieno

Lewis Research Center
Cleveland, Ohio

NATIONAL AERONAUTICS AND SPACE ADMINISTRATION • WASHINGTON, D. C. • JANUARY 1969

NASA TN D-4989

TRANSPORT STUDY OF NEUTRON AND PHOTON ATTENUATION THROUGH LITHIUM HYDRIDE AND TUNGSTEN SPHERICAL MEDIA

By John A. Peoples and Daniel Fieno

Lewis Research Center
Cleveland, Ohio

NATIONAL AERONAUTICS AND SPACE ADMINISTRATION

For sale by the Clearinghouse for Federal Scientific and Technical Information
Springfield, Virginia 22151 – CFSTI price $3.00

ABSTRACT

The S_n transport theory and a point kernel method were used to study the attenuation of (1) point fission neutrons in LiH and Li^6H, (2) point 8.00-MeV photons in tungsten, and (3) neutrons and secondary photons from a fast reactor through a laminated W-Li^6H shield. The results show that the two methods calculate in agreement neutron and photon doses through these media provided (1) at least a P_3S_{16} transport calculation is used, and (2) for neutron attenuation, the point kernel method uses a distributed neutron removal cross section for Li and Li^6 of 0.1000 cm^2/g and 0.1156 cm^2/g. Secondary photon source strength and distributions in the tungsten shells of the laminated tungsten-Li^6H shield were also determined using a P_3S_{16} transport calculation.

TRANSPORT STUDY OF NEUTRON AND PHOTON ATTENUATION THROUGH LITHIUM HYDRIDE AND TUNGSTEN SPHERICAL MEDIA

by John A. Peoples and Daniel Fieno
Lewis Research Center

SUMMARY

One-dimensional S_n transport theory and a point kernel line-of-sight method were used to study (1) the attenuation of neutrons from a point uranium-235 fission source in 117-centimeter spheres of lithium hydride (LiH) and lithium-6 hydride (Li^6H), (2) the attenuation of monoenergetic 8.00-MeV point source photons through 14 centimeters of tungsten, (3) the attenuation of neutrons and secondary photons from a fast reactor with a shield consisting of alternate layers of Li^6H and tungsten, and (4) the production of secondary gamma source strengths and distributions in the tungsten layers of the laminated shield.

The results of the study of neutron attenuation in the spheres of LiH and Li^6H showed that the two calculational methods can be made to agree provided that (1) at least a P_3S_{16} 30-group neutron transport calculation is used, and (2) the point kernel method uses neutron distributed removal cross sections for Li equal to 0.1000 square centimeter per gram and Li^6 equal to 0.1156 square centimeter per gram.

The point source study of the attenuation of 8.00-MeV photons in tungsten showed that a P_3S_{16} 16-group transport calculation was sufficient to give good agreement with the point kernel method only up to a radius of about 7 centimeters.

The calculation of the attenuation of both neutrons and secondary photons through the laminated layers of tungsten and Li^6H showed two effects. First, the calculation showed the point kernel neutron computation agreed with the P_3S_{16} 30-group transport calculation within 40 percent at a radius of 117 centimeters. This agreement was obtained using a neutron distributed removal cross section for Li^6 of 0.1156 square centimeter per gram. Second, the total secondary gamma dose rates calculated by the point kernel method and a P_3S_{16} 16-group gamma transport computation were in agreement (within 10 percent) at the outer boundary of the shield.

The transport calculations of secondary gamma ray sources in the tungsten regions of the shield, due to neutron absorption and inelastic scattering processes, were made using P_1 and P_3 elastic scattering orders and 30 and 17 neutron energy groups. The results show that for this shield configuration the influence of group structure (30 against 17) on determining source strength and distributions is negligible. However, the elastic scattering order P_3 against P_1 did show a variation in source strength for the tungsten regions being examined. The P_3 and P_1 elastic scattering orders gave essentially the same secondary production in the reflector, while in the first and second tungsten layers the results differed by 10 and 20 percent, respectively.

INTRODUCTION

Nuclear reactors for space propulsion systems or auxiliary power systems require shielding to protect personnel or system components from neutrons and gamma rays. Shielding materials must be placed so that neutron and gamma doses are within prescribed limits in various regions around the reactor. Since reactor shields are heavy, it is important that the arrangement and thicknesses of the shield materials are at a minimum weight. Two methods of calculation that are useful in the preliminary design of the shield are one-dimensional S_n transport theory and the line-of-sight point kernel method.

The S_n transport method is a numerical iterative difference method in which the continuous angular distribution of particle velocities is represented by discrete angular directions. The S_n quadrature order, which is discussed throughout this report, is a parameter related to the number of discrete angular directions. Increasing the quadrature order (S_8, S_{12}, and S_{16}) increases the number of discrete angular directions used in the problem. The elastic neutron or Compton scattering order (P_1 and P_3) denotes the spherical harmonics expansion order of the scattering source in the Boltzmann transport equation. Both types of scattering are anisotropic, therefore a number of terms in the expansion are needed to approximate the source term.

The line-of-sight point kernel method concentrates the source region into a number of individual point sources and then traces a ray from each of these point sources to a receiver point keeping track of the distance and mass thickness (g/cm^2) of each element encountered. Infinite medium buildup factors are used to calculate the gamma dose and a modified Albert Welton kernel is used to compute the fast neutron dose.

In this report the application of these methods to a number of neutron and photon shield problems is studied. A one-dimensional multigroup S_n transport code (ref. 1) is used to determine energy-dependent neutron fluxes. The fluxes are then used to compute the source of secondary gamma rays due to neutron capture and inelastic scattering processes. The S_n method is also used to determine the photon fluxes. These fluxes can then be used to determine the neutron and gamma ray doses at given detector positions in a shield. The more approximate but less complicated line-of-sight point kernel code QAD (ref. 2) is also used to compute the neutron or gamma ray doses at given detector locations. The code QAD requires known distributions of either neutron or gamma sources, gamma ray buildup factors, and neutron removal cross sections. Although high-order transport calculations, such as the S_n method, may be needed to predict accurately the doses in a shield configuration, a simpler and faster computer code such as QAD is useful for determining the effect of perturbations in shield arrangements.

The S_n approximation to the Boltzmann transport equation was studied using point isotropic uranium-235 fission sources in spheres of lithium hydride (LiH) and lithium-6 hydride (Li^6H). The S_n results for LiH were compared to Monte Carlo results. Trans-

port calculations were also performed for Li^6H because it is a shield material of interest. The effect on the calculated dose rates of varying the S_n quadrature order (n = 8, 12, and 16) and the elastic scattering order from P_1 to P_3 were also studied. The effect of neutron energy group structure was determined by varying the number of groups from 17 to 30. All of the S_n calculations included a sufficient number of mesh intervals to ensure accurate flux calculations. A number of calculations using the line-of-sight point kernel code QAD was also made to determine this code's usefulness in predicting neutron doses in these media.

The S_n transport method was also used to study the attenuation of photons in a sphere of tungsten using a point isotropic photon source having a monoenergetic energy of 8 MeV. This calculation was performed using 16 energy groups, a quadrature order of 16, and a scattering order of 3.

A P_3S_{16} transport calculation with 30 energy groups was made to compute the neutron dose of a fast reactor with a shield consisting of alternate layers of tungsten and Li^6H. Calculation of the secondary gamma ray sources in the tungsten regions of this shield, due to neutron absorption and inelastic scattering processes, was also studied using P_1 and P_3 elastic scattering orders. The gamma ray dose from the secondary gamma ray sources of this reactor was calculated using P_1S_{16} and P_3S_{16} order. Calculations of these doses for the distributed neutron and gamma ray sources were also made using the QAD code.

COMPUTER PROGRAMS AND NUCLEAR DATA

Computer Programs

Three computer programs were used to generate the necessary group-averaged microscopic and macroscopic cross sections. These programs were GAM II (ref. 3), GATHER II (ref. 4), and GAMLEG (ref. 5): GAM II is a B_3 code for the calculation of flux weighted multigroup neutron cross sections; GATHER II is used to calculate cross sections for the thermal neutron group; and GAMLEG is used to produce multigroup photon cross sections.

A one-dimensional S_n transport program (ref. 1) was used to determine neutron and photon fluxes through the various shielding materials. This program also calculated, for the case of the tungsten laminated shield, neutron absorption and inelastic reaction rates necessary to determine the secondary photon source strength and distribution.

A line-of-sight point kernel code QAD (ref. 2) was used to calculate neutron and photon dose rates. The QAD code employs infinite medium buildup factors for gamma doses and the Albert-Welton kernel for the hydrogenous material of the shield with an appropriate removal cross section for the other constituents for computing fast neutron doses.

Energy Group Structure

Two neutron energy group splits were used to describe the neutron spectra: one of 30 groups and another of 17 groups. The energy boundaries of the group structure are presented in table I. Group split A is used to give a detailed description of the high-energy part of the neutron spectrum and the resonance energy range of tungsten where some of the secondary gammas are produced by neutron absorption. Groups 2 to 10 of group split A correspond to GAM-II fine groups covering the energy range from about 4 to 10 MeV where most of the neutron dose was expected to occur. Group B is less de-

TABLE I. - NEUTRON GROUP SPLIT

(a) Group split A

Group	Boundary energy values, eV		Group	Boundary energy values, eV	
1	1.492×10^{7}	to 1.000×10^{7}	16	8.208×10^{5}	to 4.076×10^{5}
2	1.000	to 9.048×10^{6}	17	4.076	to 2.024
3	9.048	to 8.187	18	2.024	to 8.652×10^{4}
4	8.187×10^{6}	to 7.408	19	8.652×10^{4}	to 1.930
5	7.408	to 6.703	20	1.930	to 3.355×10^{3}
6	6.703	to 6.065	21	3.355×10^{3}	to 9.611×10^{2}
7	6.065	to 5.488	22	9.611×10^{2}	to 3.536
8	5.488	to 4.966	23	3.536	to 1.301
9	4.966	to 4.493	24	1.301	to 4.785×10^{1}
10	4.493	to 4.066	25	4.785×10^{1}	to 1.760
11	4.066	to 3.329	26	1.760	to 5.043×10^{0}
12	3.329	to 2.725	27	5.043×10^{0}	to 1.445
13	2.725	to 2.019	28	1.445	to 1.125
14	2.019	to 1.353	29	1.125	to 4.140×10^{-1}
15	1.353	to 8.208×10^{5}	30	4.140×10^{-1}	to 1.000×10^{-3}

(b) Group split B

Group	Boundary energy values, eV		Group	Boundary energy values, eV	
1	1.492×10^{7}	to 8.187×10^{6}	10	3.355×10^{3}	to 5.829×10^{2}
2	8.187×10^{6}	to 5.488	11	5.829×10^{2}	to 1.013
3	5.488	to 3.012	12	1.013	to 2.902×10^{1}
4	3.012	to 1.353	13	2.902×10^{1}	to 1.068
5	1.353	to 9.072×10^{5}	14	1.068	to 3.059×10^{0}
6	9.072×10^{5}	to 4.076	15	3.059×10^{0}	to 1.125
7	4.076	to 1.111	16	1.125	to 4.140×10^{-1}
8	1.111	to 1.503×10^{4}	17	4.140×10^{-1}	to 1.000×10^{-3}
9	1.503×10^{4}	to 3.355×10^{3}			

TABLE II. - GAMMA GROUP SPLIT

(a) Group split A

Group	Boundary energy value, eV	Group	Boundary energy value, eV
1	8.25×10^6 to 7.75×10^6	9	3.00×10^6 to 2.60×10^6
2	7.75 to 6.75	10	2.60 to 2.20
3	6.75 to 5.50	11	2.20 to 1.80
4	5.50 to 5.00	12	1.80 to 1.35
5	5.00 to 4.50	13	1.35 to 9.00×10^5
6	4.50 to 4.00	14	9.00×10^5 to 4.00
7	4.00 to 3.50	15	4.00 to 2.60
8	3.50 to 3.00	16	2.60 to 1.00

(b) Group split B

Group	Boundary energy value, eV	Group	Boundary energy value, eV
1	8.00×10^6 to 5.50×10^6	8	2.60×10^6 to 2.20×10^6
2	5.50 to 5.00	9	2.20 to 1.80
3	5.00 to 4.50	10	1.80 to 1.35
4	4.50 to 4.00	11	1.35 to .90
5	4.00 to 3.50	12	.90 to .40
6	3.50 to 3.00	13	.40 to .260
7	3.00 to 2.60	14	.260 to .10

tailed and was used in the interest of reducing computer run time. The thermal group of both group structures (A and B) extends from 0.001 to 0.414 electron volt.

For the analysis of photon attenuation, the two energy group splits shown in table II were used. Group split A was used in the calculation of the 8.00-MeV monoenergetic point gamma source. Group split B was used in the gamma transport calculation through the laminated shield. Group splits A and B differ only in that the first group of group split B was divided into three groups to provide a more adequate group structure for the point source calculation.

Secondary Photon Spectra

The use of tungsten as a shield against primary photons is highly effective; however, in the neutron flux field of a reactor this material gives rise to a considerable source of secondary gamma radiation. These secondary photons are a consequence of neutron absorptions and inelastic scattering interactions with the tungsten nuclei. The secondary photon spectra for tungsten absorptions and inelastic scattering events are given in

TABLE III. - SECONDARY PHOTON SPECTRA

FOR TUNGSTEN

Energy group, Mev	Absorption spectra, MeV/absorption	Inelastic spectra, MeV/inelastic scattering
8.00 to 5.50	0.720	0.002
5.50 to 5.00	.320	.002
5.00 to 4.50	.260	.002
4.50 to 4.00	.200	.002
4.00 to 3.50	.750	.002
3.50 to 3.00	.750	.005
3.00 to 2.60	.580	.020
2.60 to 2.20	.580	.030
2.20 to 1.80	.650	.060
1.80 to 1.35	.450	.700
1.35 to .90	.500	1.000
.90 to .40	.490	.050
.40 to .26	.120	.050
.26 to .10	.00	.00

table III. These spectra were derived from the data of reference 6. No secondary photon sources other than tungsten were considered in this study.

Dose Conversion Factors

Two sets of neutron flux conversion factors were used: (1) the Hurst single scatter factors presented in reference 7, and (2) the first collision factors given in reference 8. These neutron dose conversion factors are listed in table IV for the two energy group splits A and B. The gamma flux conversion factors to rad per hour, shown in table V, were calculated using the photon energy absorption coefficients obtained from reference 9.

TABLE IV. - NEUTRON FLUX TO DOSE CONVERSION

(a) Group split A

Group	First collision conversion, rad/hr / neutron/(cm^2)(sec)	Hurst conversion, mrep/hr / neutron/(cm^2)(sec)	Group	First collision conversion, rad/hr / neutron/(cm^2)(sec)	Hurst conversion, mrep/hr / neutron/(cm^2)(sec)
1	2.00×10^{-5}	1.60×10^{-2}	16	6.30×10^{-6}	6.50×10^{-3}
2	1.80	↓	17	5.04	3.20
3	1.76		18	2.88	0
4	1.73		19	1.44	↓
5	1.69		20	0	
6	1.62		21	↓	
7	1.58		22		
8	1.55		23		
9	1.44		24		
10	1.40		25		
11	1.35		26		
12	1.30	1.40×10^{-2}	27		
13	1.19	1.25	28		
14	9.90×10^{-6}	1.08	29		
15	8.28	8.80×10^{-3}	30		

(b) Group split B

Group	First collision conversion, rad/hr / neutron/(cm^2)(sec)
1	2.00×10^{-5}
2	1.70
3	1.48
4	1.08
5	8.40×10^{-6}
6	6.40
7	3.61
8	1.18×10^{-7}
9	0
10	↓
11	
12	
13	
14	
15	
16	
17	

TABLE V. - GAMMA FLUX TO DOSE CONVERSION

(a) Group split A

Group	Gamma conversion, rad/hr / photon/(cm^2)(sec)	Group	Gamma conversion, rad/hr / photon/(cm^2)(sec)
1	7.828×10^{-6}	9	3.697×10^{-6}
2	7.250	10	3.222
3	6.430	11	2.913
4	5.712	12	2.472
5	5.345	13	1.883
6	4.895	14	1.105
7	4.513	15	5.886×10^{-7}
8	4.102	16	3.240

(b) Group split B

Group	Gamma conversion, rad/hr / photon/(cm^2)(sec)	Group	Gamma conversion, rad/hr / photon/(cm^2)(sec)
1	6.510×10^{-6}	8	3.322×10^{-6}
2	5.712	9	2.913
3	5.345	10	2.472
4	4.895	11	1.883
5	4.513	12	1.105
6	4.102	13	5.886×10^{-7}
7	3.697	14	3.240

POINT SOURCE ANALYSIS

Neutron Attenuation - Lithium Hydride Spheres

The LiH medium was used to examine the effect on neutron dose of varying the S_n quadrature order, the elastic scattering order, and energy group structure. Since high-order S_n transport problems require longer computer running times, it is worthwhile to investigate the effect of lower order calculations on dose in an effort to conserve computer run time.

The study used a point uranium-235 fission source of neutrons in spheres of LiH and Li^6H with densities of 0.750 and 0.6614 gram per cubic centimeter, respectively. Figures 1 and 2 show the results on neutron dose rate of a P_3 17 group transport calculations with varying quadrature order from S_{16} to S_8 in 117-centimeter radii sphere of LiH and Li^6H. These data indicate that the transport results for dose rate have converged at an S_n order of 16 for neutron penetrations up to 117 centimeters. Decreasing the S_n order to 12 or even 8 decreases the calculated neutron dose rate at the 117-

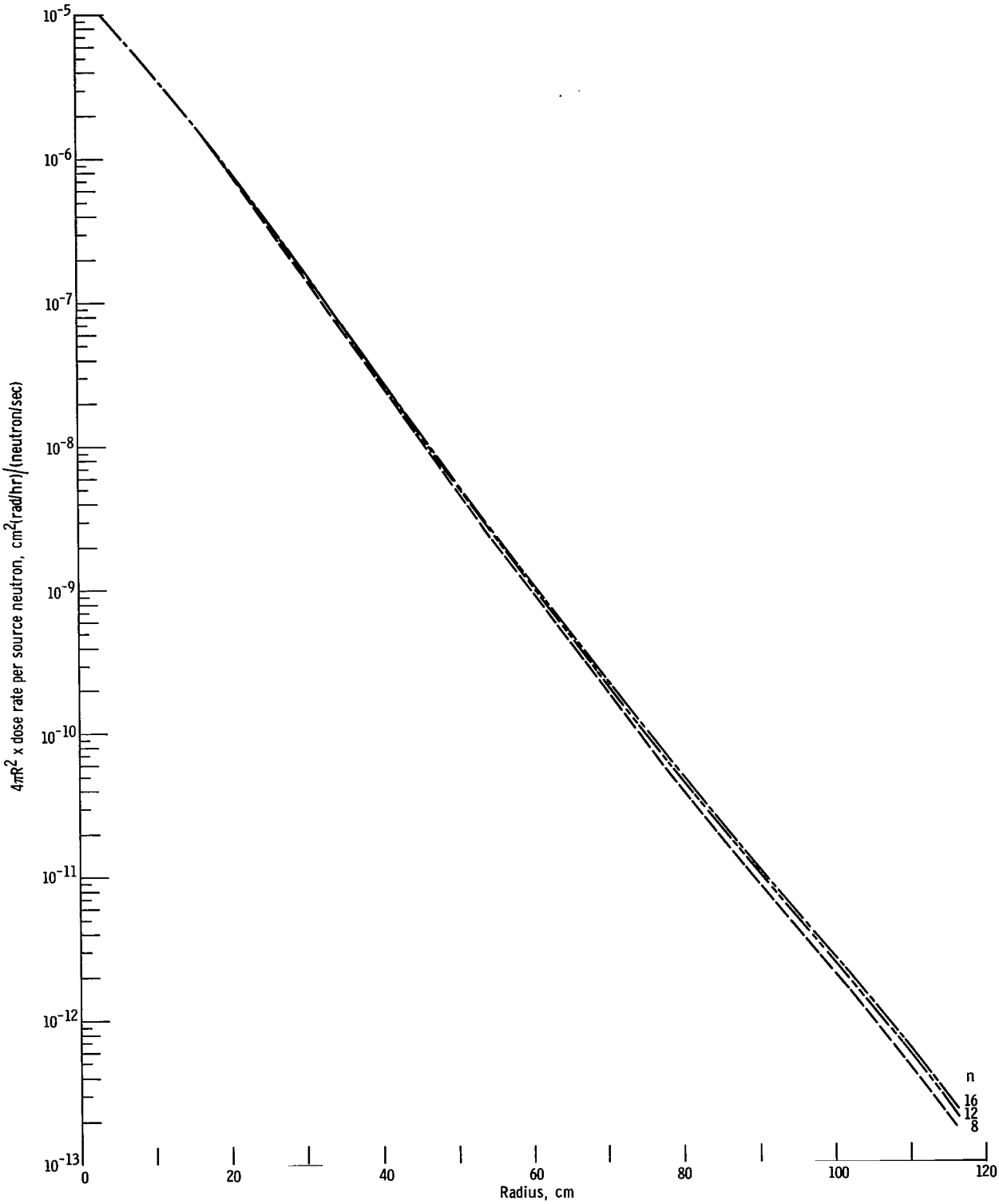

Figure 1. - Variation of neutron dose rate through lithium hydride sphere as function of S_n order (n = 8, 12 or 16). Point uranium-235 fission source; 17 neutron energy groups; elastic scattering order P_3.

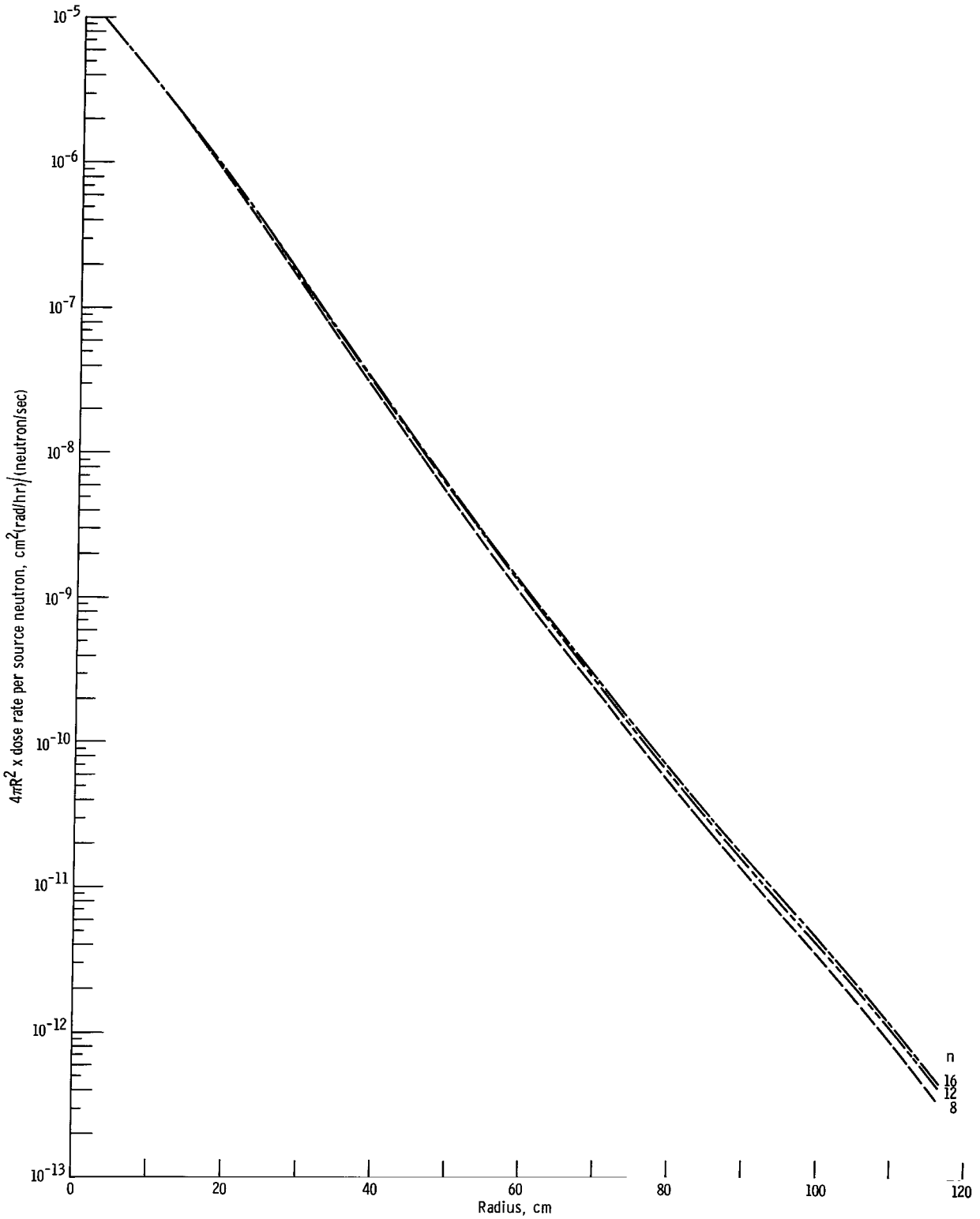

Figure 2. - Variation of neutron dose rate through lithium-6 hydride sphere as function of S_n order (n = 8, 12 or 16). Point uranium-235 fission source; 17 neutron energy groups; elastic scattering order P_3.

TABLE VI. - RELATIVE FLUX VALUES FOR VARYING S_n AND ELASTIC SCATTERING ORDERS THROUGH A LITHIUM HYDRIDE MEDIUM WITH 17 NEUTRON ENERGY GROUPS

[Boundary energy values: 14.92 to 8.187 MeV for group 1; 3.01 to 1.35 MeV for group 4; and 0.407 to 0.111 MeV for group 7.]

S_n calculation order	Radius, r = 20 cm			Radius, r = 70 cm			Radius, r = 117 cm		
	Group 1	Group 4	Group 7	Group 1	Group 4	Group 7	Group 1	Group 4	Group 7
P_3S_8	8.342×10^{-8}	5.039×10^{-6}	4.821×10^{-6}	1.268×10^{-11}	7.32×10^{-11}	5.750×10^{-11}	1.163×10^{-14}	1.947×10^{-14}	1.000×10^{-14}
P_3S_{12}	8.566	5.206	4.950	1.462	8.31	6.482	1.437	2.348	1.200
P_3S_{16}	8.601	5.177	4.969	1.569	8.85	6.885	1.592	2.583	1.317
P_1S_{16}	1.038×10^{-7}	5.420	3.167	1.977	8.067	3.975	1.925	2.522	8.30

centimeter position of the sphere by as much as 10 to 25 percent. The S_n quadrature coefficients used for this study were moments-modified ordinates and weights.

Although the doses may have converged, the fluxes may not be completely converged. Table VI shows the relative flux values for this series of transport calculations at various radii through the spherical medium. At a radius of 117 centimeters, the flux values for the three representative neutron groups are not completely converged at S_{16}.

The next consideration was the determination of the effect on dose when the elastic scattering order is varied. The S_n quadrature order was held constant at 16 while the elastic scattering order was changed from P_3 to P_1, again with the point fission source in LiH. The P_1S_{16} 17-group transport calculation was then compared with the P_3S_{16} computation and the data plotted in figure 3. At 110 centimeters, the P_3S_{16} calculations show a resulting dose rate almost twice the value of the P_1S_{16} computation. Calculations with higher order elastic scattering were not performed because the GAM II cross section code is limited to a P_3 scattering order computation. However, reference 10 shows that for deep (120-cm) penetration of neutrons in water, the dose values have converged at the P_3 scattering order.

Finally, the effect of varying neutron group structure on dose rate was examined. A comparison was made between a 17- and 30-group structure (see table I) problem. A dose rate was computed with the 30 broad neutron groups and the same point fission source in a LiH sphere using a P_3S_{16} transport calculation. The results are shown in figure 3. At 116 centimeters, near the outer boundary of the LiH sphere, the 30-group dose rate calculation gave results more than twice that of the corresponding 17-group computation.

The large difference in the doses with 30 energy groups and 17 energy groups is due, in part, to the cross-section averaging procedure used by the GAM-II computer code. GAM-II generates an infinite medium flux spectrum for given input source spectrum and material composition. This flux spectrum is then used to average the 99 GAM-II fine

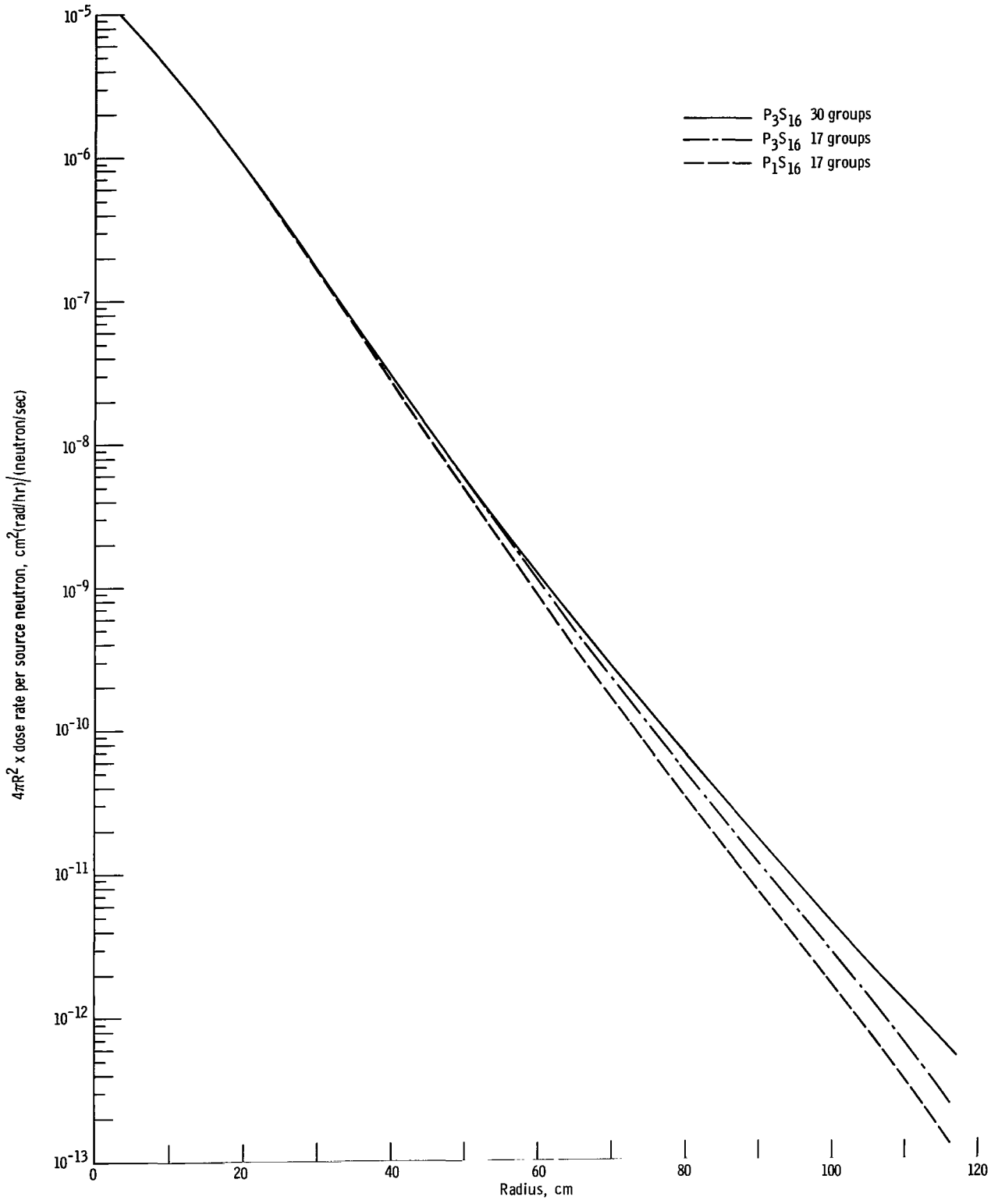

Figure 3. - Dose rate variation with elastic scattering order (P_1 or P_3) and neutron energy group structure through lithium hydride sphere for a point source of uranium-235 fission neutrons.

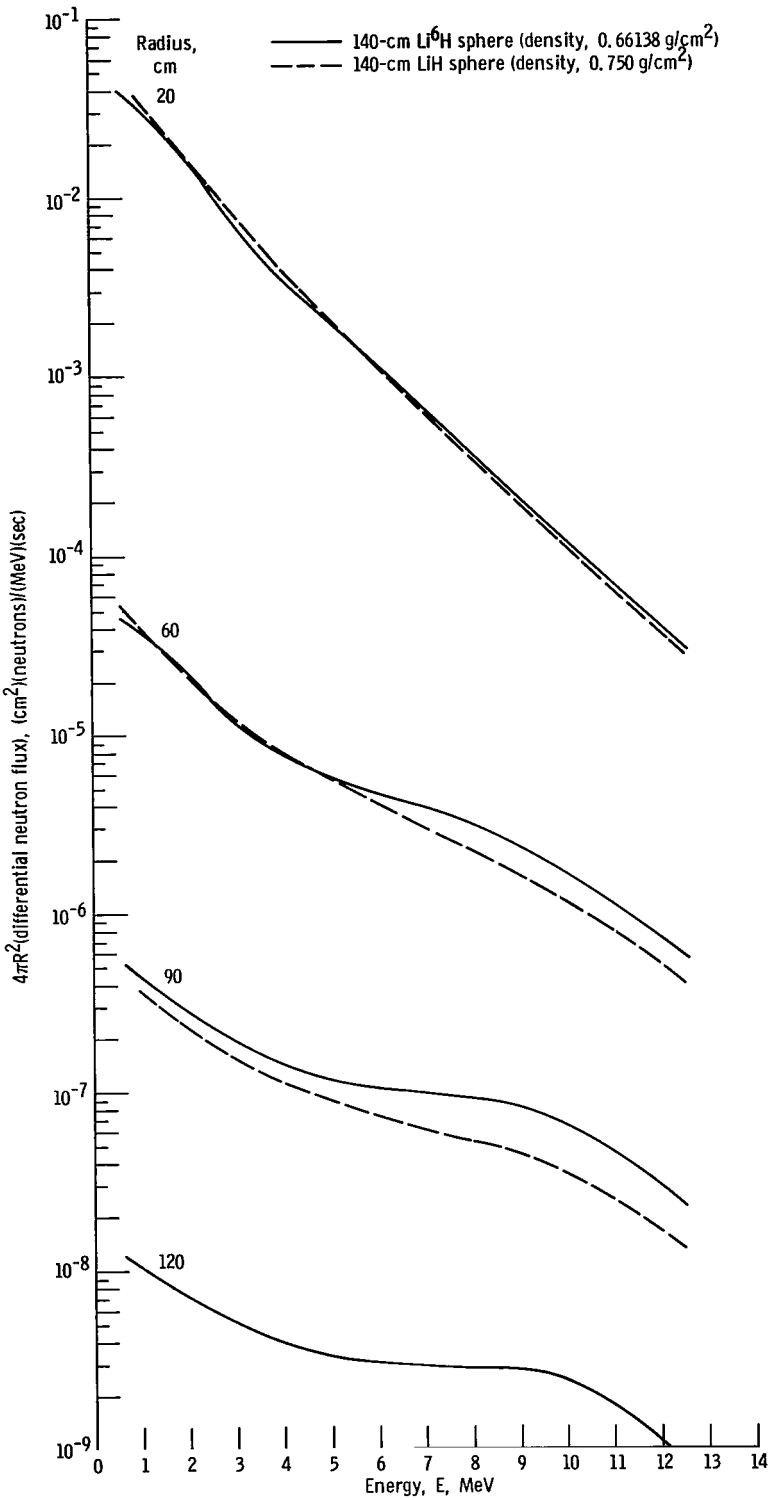

Figure 4. - Neutron spectrum through spheres of lithium hydride and lithium-6 hydride. Point uranium-235 fission source; 30 neutron groups; P_3S_{16} S_n transport.

group structure so that cross sections for various broad group energy structures can be obtained. The spectrum in the LiH far from the source becomes much harder (i.e., the average energy of the spectrum increases) than even the uranium-235 fission spectrum. Thus, averaging over infinite medium spectra may be inappropriate for these calculations. However, it is expected that the more detailed 30-group split is less sensitive than the corresponding 17-group split to the method of averaging the neutron cross sections. This hardening effect is shown in figure 4 for the point uranium-235 fission spectrum calculations in spheres of LiH and Li^6H. The differential neutron number (neutrons/(MeV)(sec)) is plotted as a function of energy at various positions in spheres of LiH and Li^6H for the two energy group splits. From these figures the distinct flattening of the spectral curves is seen at the 90- and 120-centimeter positions. The average energies of these spectra at various positions are given in table VII.

TABLE VII. - AVERAGE ENERGIES OF NEUTRONS IN LiH AND Li^6H FOR A POINT ISOTROPIC FISSION SOURCE (30 GROUPS)

Radius, cm	Average energy, E, MeV	
	LiH	Li^6H
0	2.00	2.00
20	1.82	1.91
60	2.67	2.99
90	3.64	4.13
120	4.20	4.67

Figure 5 is a comparison of a 30-group P_3S_{16} transport calculation and a QAD point kernel computation of neutron dose through LiH with Kam's Monte Carlo results (ref. 11). Though the S_n transport differs with the Monte Carlo results at 90 centimeters, the S_n data do fall within the three sigma error bar of the Monte Carlo calculation. The differences between the S_n and Monte Carlo results can be due to differences in the fine group neutron cross sections used by these two methods, the inadequacy of the GAM II cross-section averaging process, too few broad neutron groups used for the S_n calculation and to the choice of the moments-modified S_n quadrature set.

The QAD data shown in figure 5 are the result of using two neutron removal cross sections for natural lithium and the following modified Albert-Welton coefficients (ref. 12):

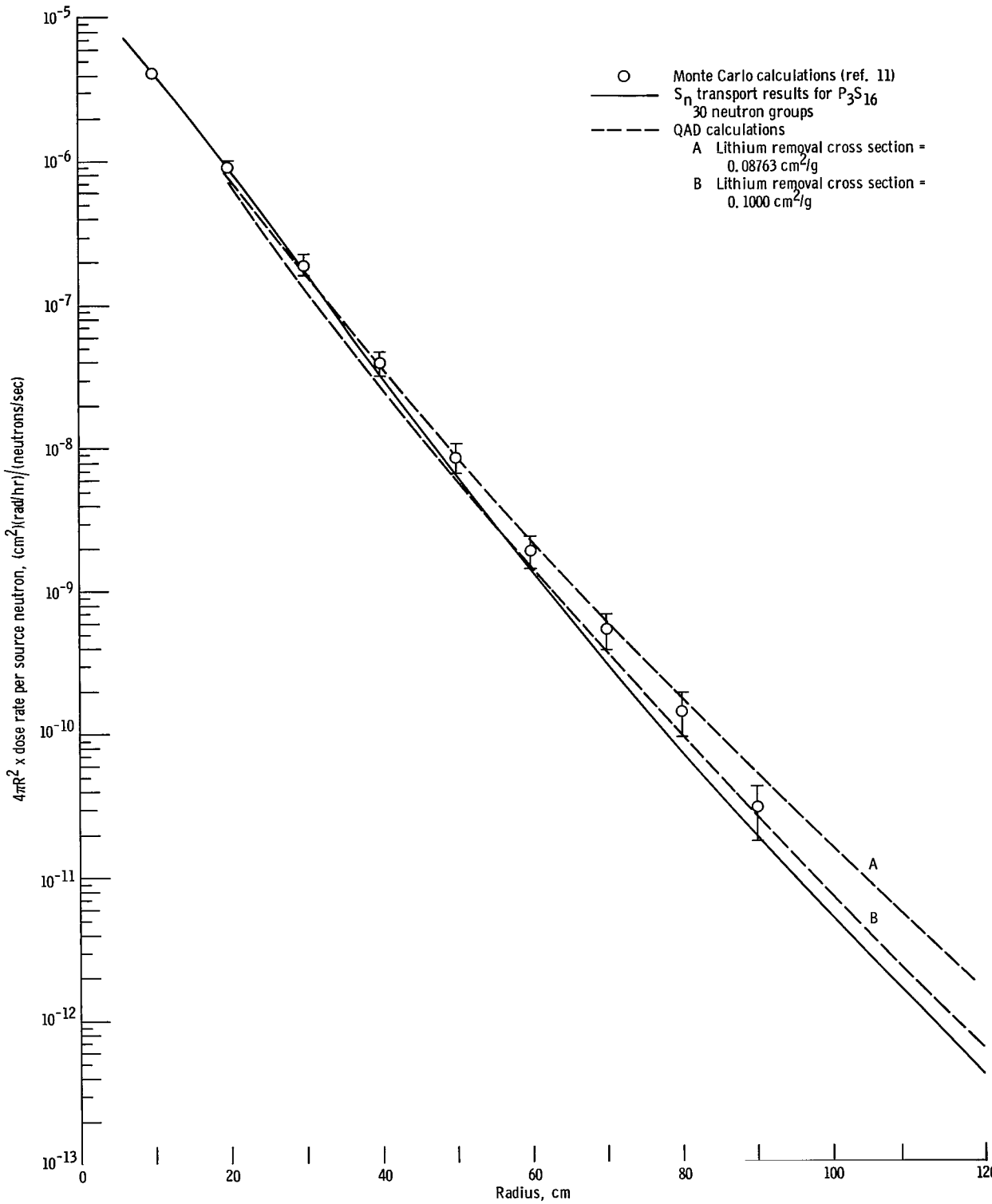

Figure 5. - Comparison of 30-group P_3S_{16} transport, QAD, and Monte Carlo calculations of the neutron dose rates in lithium hydride sphere for a point source of uranium-235 fission neutrons.

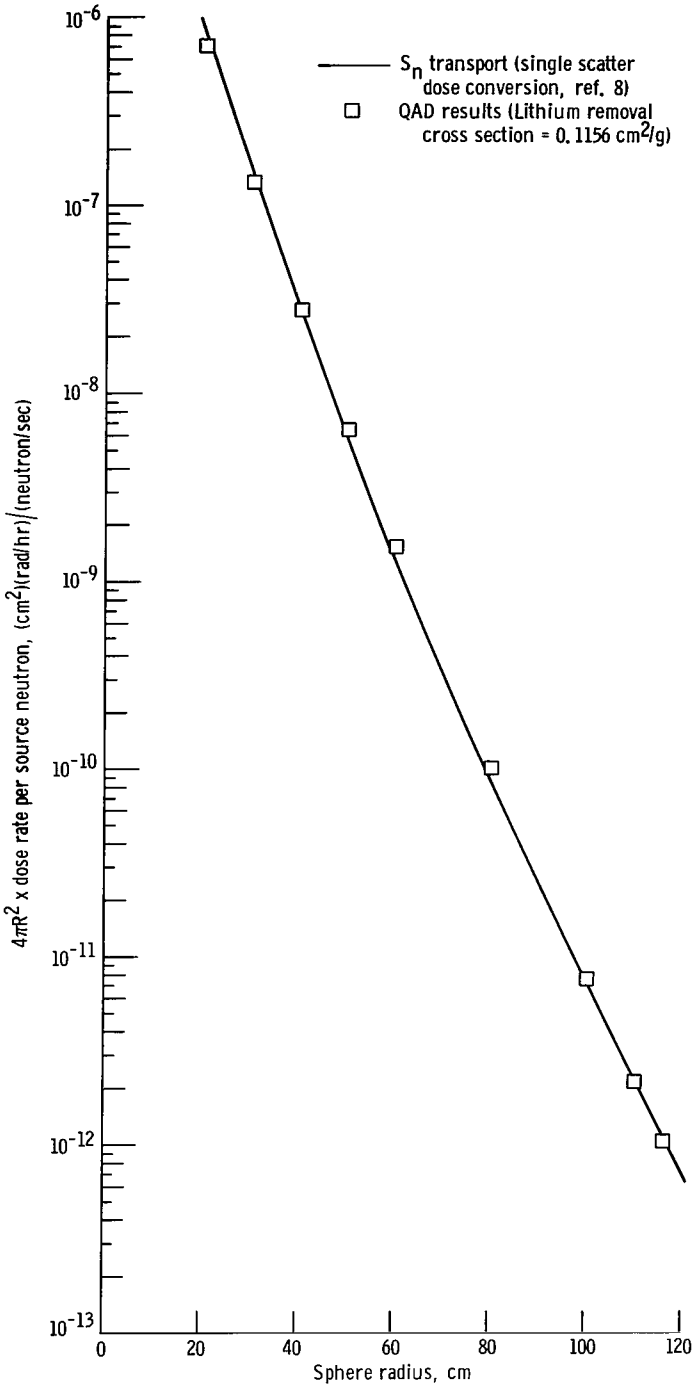

Figure 6. - Comparison of 30-group P_3S_{16} transport and QAD neutron dose rates through lithium-6 hydride (density, 0.66138 g/cm^3) for a point source of uranium-235 fission neutrons.

α_1 . . . . . 7.29×10^9 mrep/(hr-W)cm^2
α_2 . . . . . 0.290
α_3 . . . . . 0.830
α_4 . . . . . 0.580

Curve A uses the slab removal cross section for lithium of 0.0876 square centimeter per gram obtained from reference 12. Curve B uses a distributed removal cross section of 0.100 square centimeter per gram obtained by fitting the removal cross section for lithium to the S_n transport data. Reference 13 presents a more detailed discussion for obtaining distributed neutron removal cross sections for lithium and lithium-6.

Figure 6 shows the results of an S_n transport and QAD calculation of point source neutron attenuation in a sphere of Li^6H. The good agreement established between the S_n transport and the QAD calculation is the result of correcting the neutron removal cross section for lithium. A correction was made to the distributed removal cross section (0.100 cm^2/g) determined in the preceding LiH study to account for the difference in density between natural lithium and lithium-6. Since the overall scattering cross sections for lithium and lithium-6 are quite similar, this density correction to the neutron removal cross section has proved to be adequate. The value used in the QAD calculation of figure 6 to represent the distributed removal cross section for lithium-6 was 0.1156 square centimeter per gram.

Photon Attenuation - Tungsten Sphere

The S_n transport calculations were made for a point monoenergetic photon source of 8.00 MeV in an 18-centimeter tungsten sphere. The tungsten density was taken as 19.3 grams per cubic centimeter. The photon dose rates calculated by this method were compared, at various positions through the tungsten, with the moments method results reported by Goldstein and Wilkens (ref. 14). The point kernel code (QAD) gives the same results as the moments method. The S_n transport calculation used to study this problem had 16 photon energy groups (see table II), an S_n order of 16, and P_3 and P_1 Compton scattering orders. The energy group spacing of 16 was considered detailed enough in the high-energy region to be adequate for this photon study.

The dose rates generated by the two calculational method (moments and transport) are shown in figure 7. Good agreement is found between the two methods up to approximately 7 centimeters of tungsten. At this point, the P_3S_{16} transport calculation begins to diverge from the moments method.

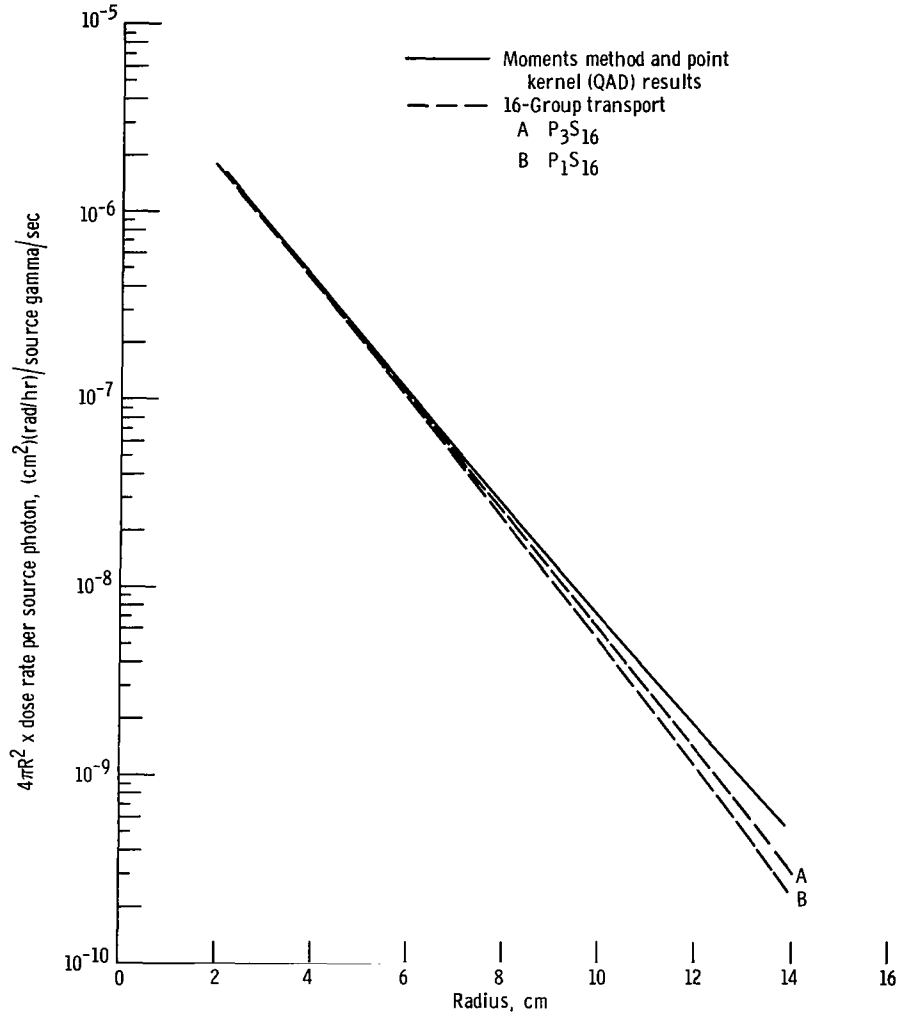

Figure 7. - Comparison of dose rates calculated by S_n transport and moments methods for 8.00-MeV point source in tungsten sphere.

LAMINATED SHIELD ANALYSIS

The final portion of this study examines a spherical reactor-laminated shield combination. A 2.5-megawatt (thermal power) fast reactor was enclosed in a 4π laminated tungsten-Li^6H shield. The reactor core and reflector composition are given in table VIII. This reactor configuration was chosen because the neutron and photon attenuation problems are similar to those that might be encountered in a typical space power reactor shield (ref. 15).

TABLE VIII. - SIZE AND COMPOSITION OF REACTOR AND SHIELD

Region	Radius		Element	Atom density, atom/(b)(cm)
	Inner, cm	Outer, cm		
1	0	18.00	U-233 W Li^7 O	0.009357 .026849 .004686 .018897
2	18.00	29.00	W Li^7	0.06022 .002343
3	29.00	36.62	H, Li^6 } Li^6H	0.056837 .056837
4	36.62	46.78	W	0.0632
5	46.78	54.40	H, Li^6 } Li^6H	0.056837 .056837
6	54.40	56.94	W	0.0632
7	56.94	117	H, Li^6 } Li^6H	0.056837 .056837

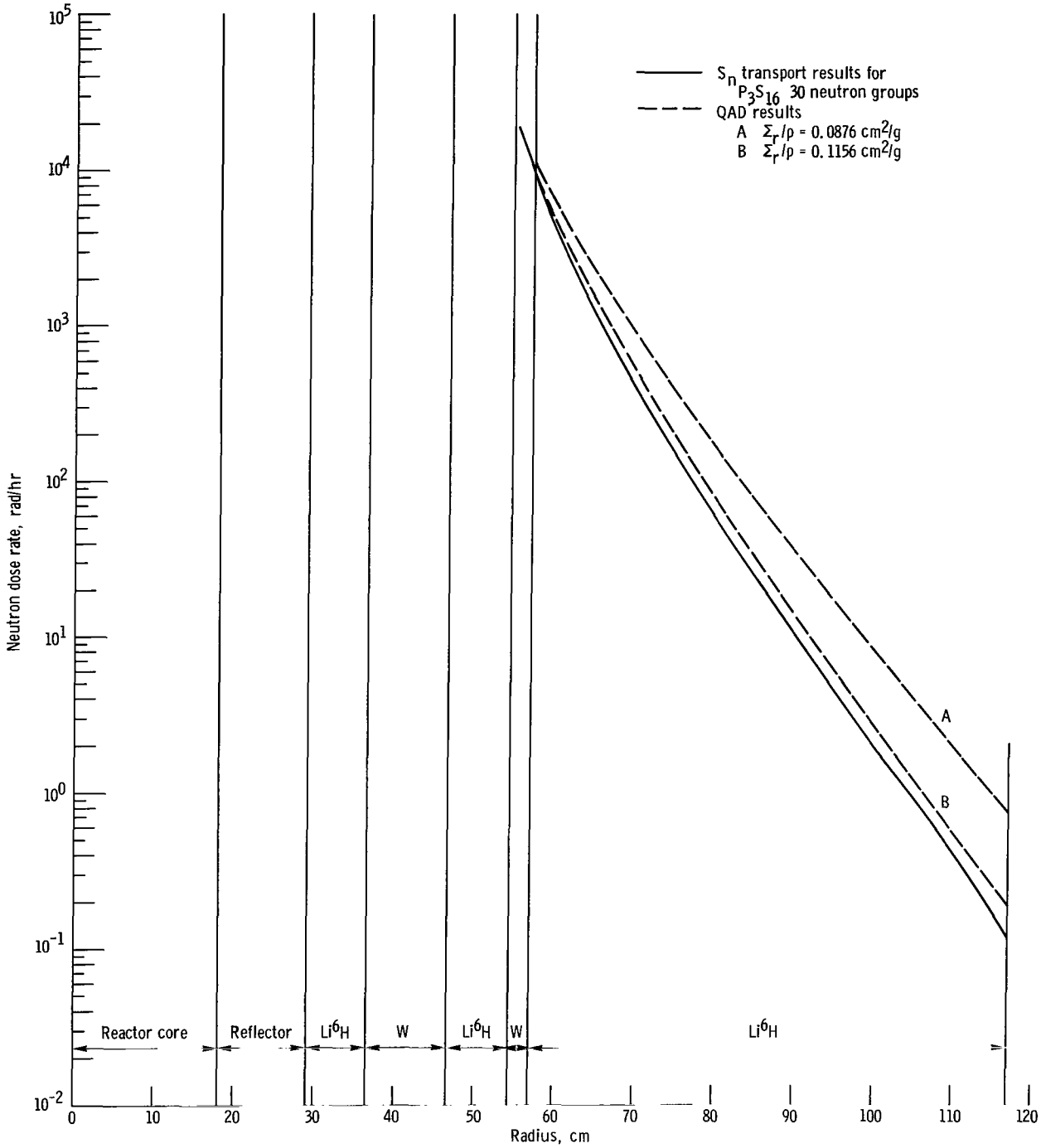

Figure 8. - Comparison of neutron dose rates in laminated shield for 30-group P_3S_{16} transport computation and QAD calculation for the model fast reactor.

Neutron Dose Analysis

The initial portion of this analysis will be concerned with the neutron dose rate from the model reactor-laminated shield. From the point source study, it was decided to use a P_3S_{16} 30-group transport calculation for the laminated shield.

Figure 8 is a comparison of a 30-group P_3S_{16} transport calculation and two QAD computations of the neutron dose in the laminated shield. The dotted curves A and B are QAD calculations for two values of the neutron removal cross section for lithium. Curve A uses the lithium slab removal cross section of 0.0876 square centimeter per gram. These data show that by using this value for removal cross sections the results may differ from the S_n transport data by as much as a factor of 6 at a radius of 117 centimeters in the shield. Curve B utilizes the removal cross section for lithium of 0.1156 square centimeter per gram as determined in the preceding point source analysis. These results show that the QAD and S_n transport calculations differ by only 50 percent at a radius of 117 centimeters. For both of these QAD calculations, the neutron removal cross section used for tungsten was 0.0110 square centimeter per gram.

Secondary Gamma Source Analysis

The final analysis of this study will examine the major contributor to the dose rate emanating from this shield. The secondary gammas produced by tungsten neutron absorptions and inelastic scatterings result in dose rates several orders of magnitude greater than the dose from the primary core gammas. The tungsten reflector used in this reactor configuration is thick enough to significantly reduce the importance of the primary gammas and these will warrant no further discussion. Other possible sources of secondary gammas such as Li^6H will also be neglected.

The calculational procedure used to determine the dose rates from these secondary sources is as follows:

(1) The total number of absorptions and inelastic scattering (events/(cm^3)(sec/source neutron)) is first determined for the tungsten regions by an S_n neutron transport calculation. The results are then used to evaluate a total photon source strength and spatial distribution for each tungsten region.

(2) These computed strengths and distributions are then used by either QAD or the S_n transport calculation to determine the dose of these secondary gammas through the remainder of the shield.

From the S_n transport calculations it was found that a variation in elastic scattering order (P_1 or P_3) influenced the total number of absorptions and inelastic scattering events calculated for the tungsten regions. A variation in energy group structure was

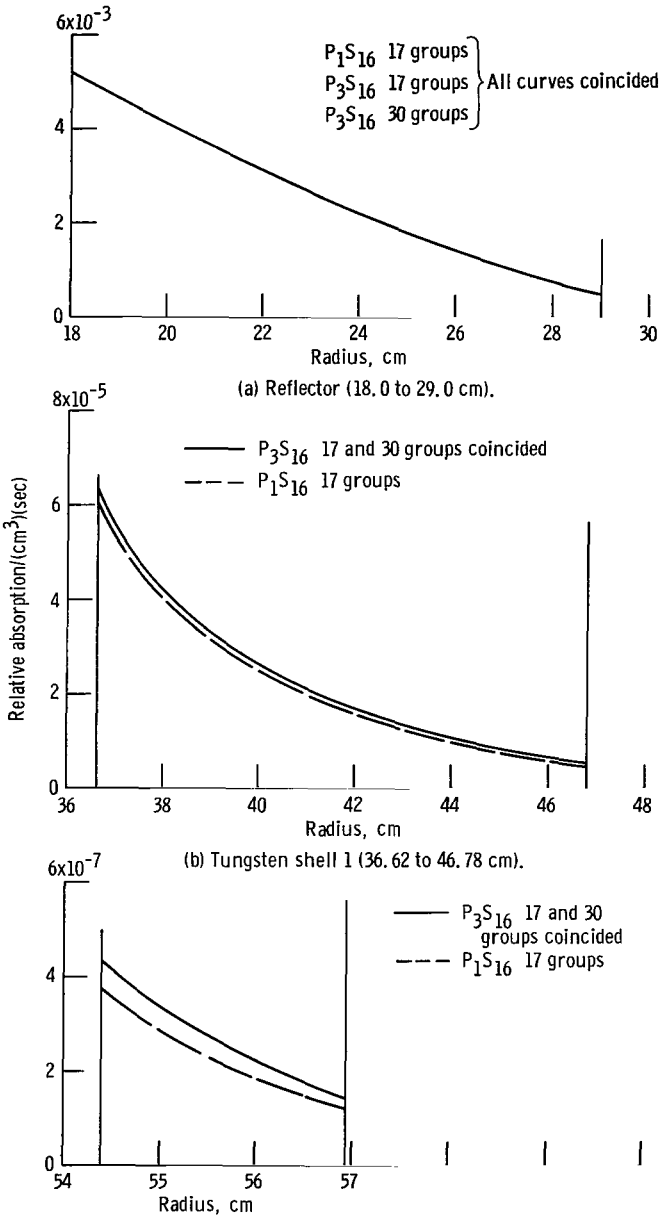

Figure 9. - Relative distribution of absorptions in tungsten regions of model fast reactor and shield.

also studied. Changing the total number of energy groups from 17 to 30 had little effect on either the secondary gamma source strength or distribution.

Figures 9 and 10 show the relative distribution of absorptions and inelastic interactions in the reflector, first tungsten region, and in the final tungsten region for P_3S_{16} (17- and 30-group) and a P_3S_{16} (17-group) transport calculations. As can be seen from these figures, the relative distributions for both absorptions and inelastic scattering events are for the most part the same for either the 30-group neutron structure or the

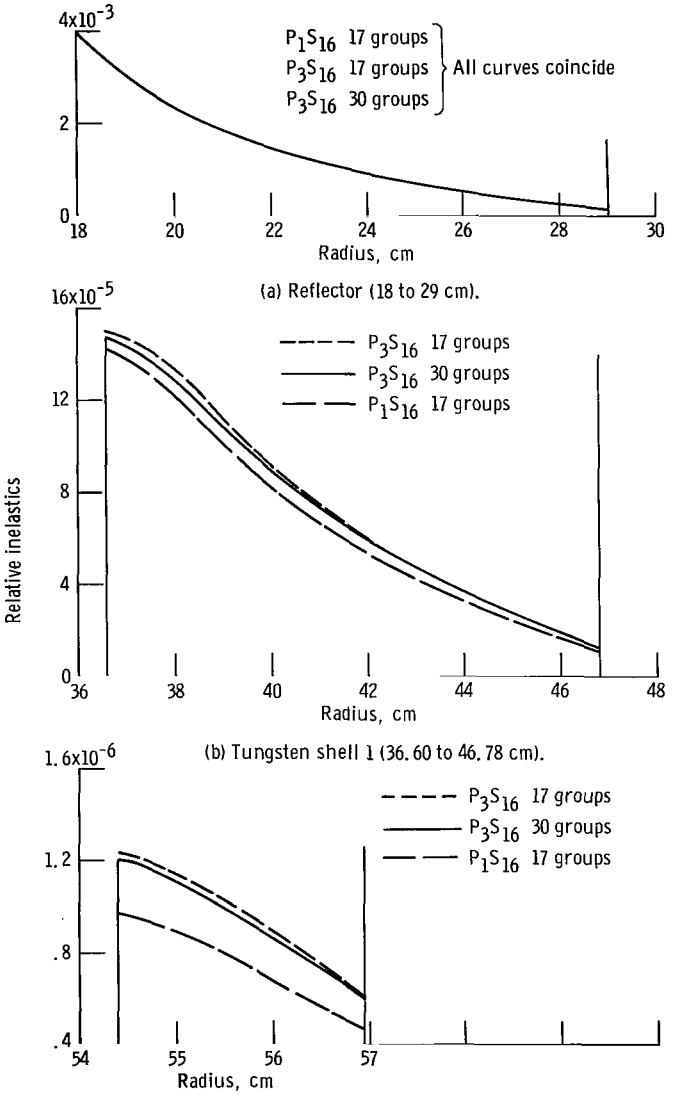

Figure 10. - Relative distribution of inelastic scattering events in tungsten regions of the model fast reactor and shield.

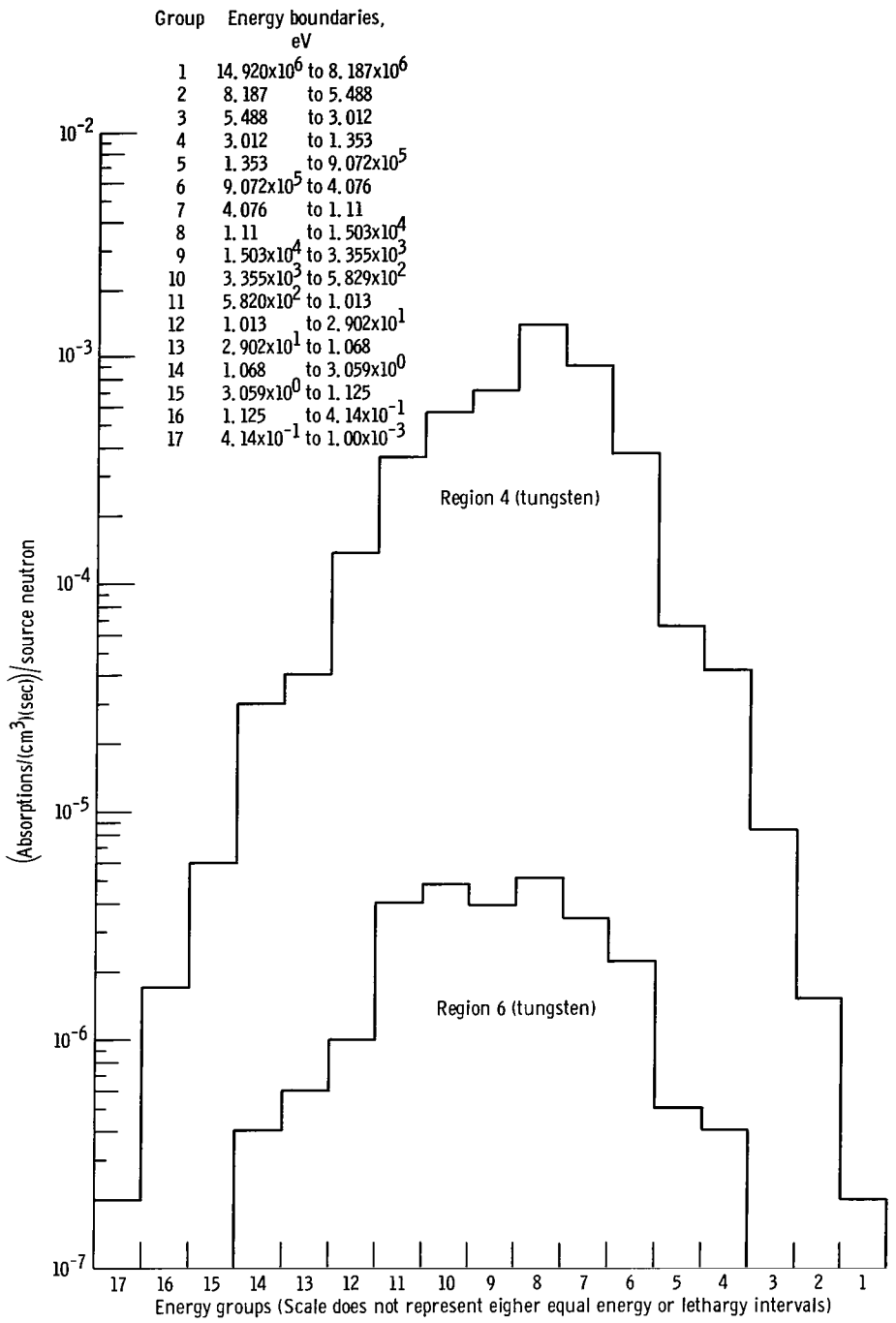

Figure 11. - Absorptions as function of energy group within two tungsten shells as determined by P_1S_{16} and P_3S_{16} transport calculations for model fast reactor.

17-group structure. The P_1 and P_3 elastic scattering order gives essentially the same secondary production in the reflector, in the first tungsten layer they differ by about 10 percent, and in the final tungsten layer the difference amounts to about 20 percent.

Figures 11 and 12 show the absorptions and inelastic scattering events as functions of neutron energy for the reflector and two tungsten regions of the laminated shield for the 17 neutron energy group split. From figure 11 it can be seen that a large portion of the absorptions take place in energy groups 6 to 12 (907 keV to 29 eV) with the maximum occurring in group 8 (111.1 to 15 keV). From figure 12 it can be seen that a large portion of the inelastic scattering events take place in energy groups 3 to 7 (5.49 to 4.08 meV).

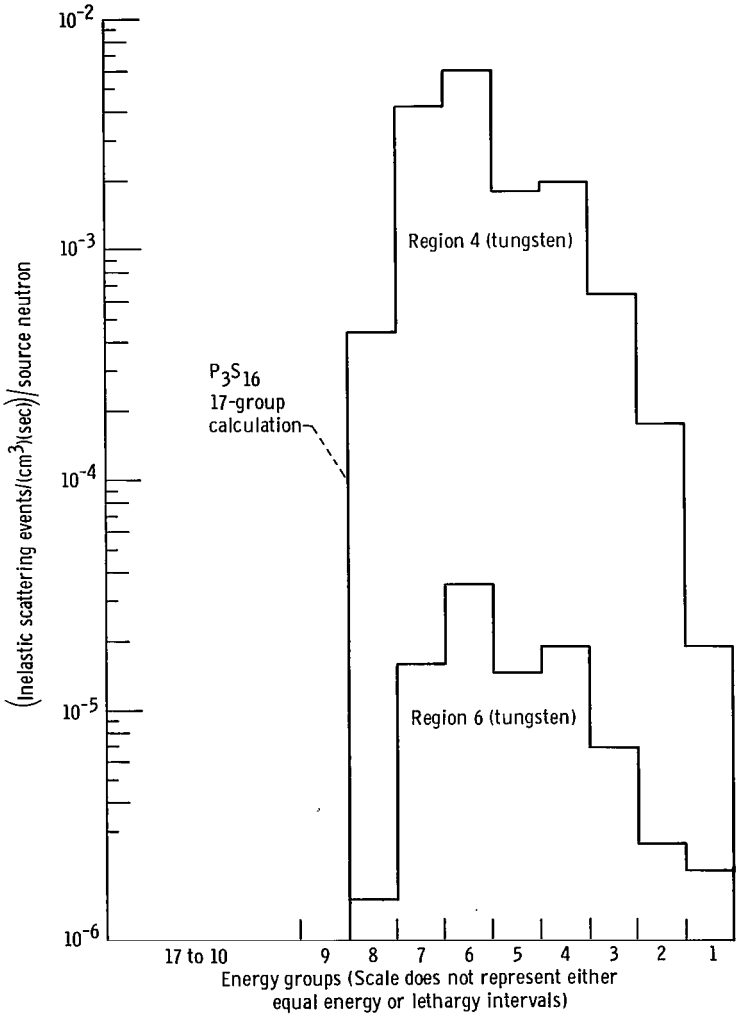

Figure 12. - Tungsten inelastic scattering events as function of energy group within two tungsten shells for model fast reactor.

Secondary Gamma Dose Analysis

The variation in source strength and source distribution due to the changing of elastic scattering order and, to a small degree, neutron group structure, can be seen more clearly when the dose rates resulting from the use of these sources are compared. Using the absorption and inelastic gamma spectra shown in table III enables the determination of the gamma dose rates by an S_n photon transport calculation. Table IX shows the total secondary dose rate at the periphery of the laminated shield and the individual contributions to the total dose from the reflector and each of the tungsten regions. Figure 13 is a plot of the secondary gamma dose rates from each of the tungsten regions throughout the laminated shield. These data are generated using a P_3S_{16} 14-group transport calculation. The secondary source strength and source distributions for each of these regions were generated by a P_3S_{16} 17-group neutron transport calculation.

The QAD results are also given in table IX for comparison purposes. The total secondary gamma dose rates calculated by QAD are in good agreement with the S_n transport calculation. However, the gamma dose contribution from the reflector, as calculated by the S_n transport method and the QAD code, differs considerably. Since both codes used the same secondary source strengths and source distributions, the difference must lie

TABLE IX. - SECONDARY GAMMA DOSE RATES FOR THE TUNGSTEN REFLECTOR AND TUNGSTEN SHIELD COMPONENTS (DETECTOR LOCATED AT 117 CM)

Source generation calculation	Gamma transport calculation	Radiation type	Dose rates, rad/hr at detector			Dose rate for detector at 117 cm, rad/hr	Total dose
			Region 2	Region 4	Region 6		
P_1S_{16} (17 group)	P_1S_{16} (14 group)	Absorption	0.167	24.230	10.170	34.567	54.712
		Inelastic	.025	10.440	9.680	20.145	
	QAD	Absorption	0.555	28.660	10.490	39.705	62.013
		Inelastic	.098	12.880	9.330	22.308	
P_3S_{16} (17 group)	P_3S_{16} (14 group)	Absorption	0.304	28.230	11.780	40.314	66.094
		Inelastic	.050	13.370	12.360	25.780	
	QAD	Absorption	0.552	31.400	12.840	44.792	71.999
		Inelastic	.097	14.810	12.300	27.207	
P_3S_{16} (30 group)	P_3S_{16} (14 group)	Absorption	0.316	27.510	11.600	39.426	65.236
		Inelastic	.050	13.260	12.500	25.810	
	QAD	Absorption	0.551	30.390	12.890	43.831	70.739
		Inelastic	.098	14.460	12.350	26.908	

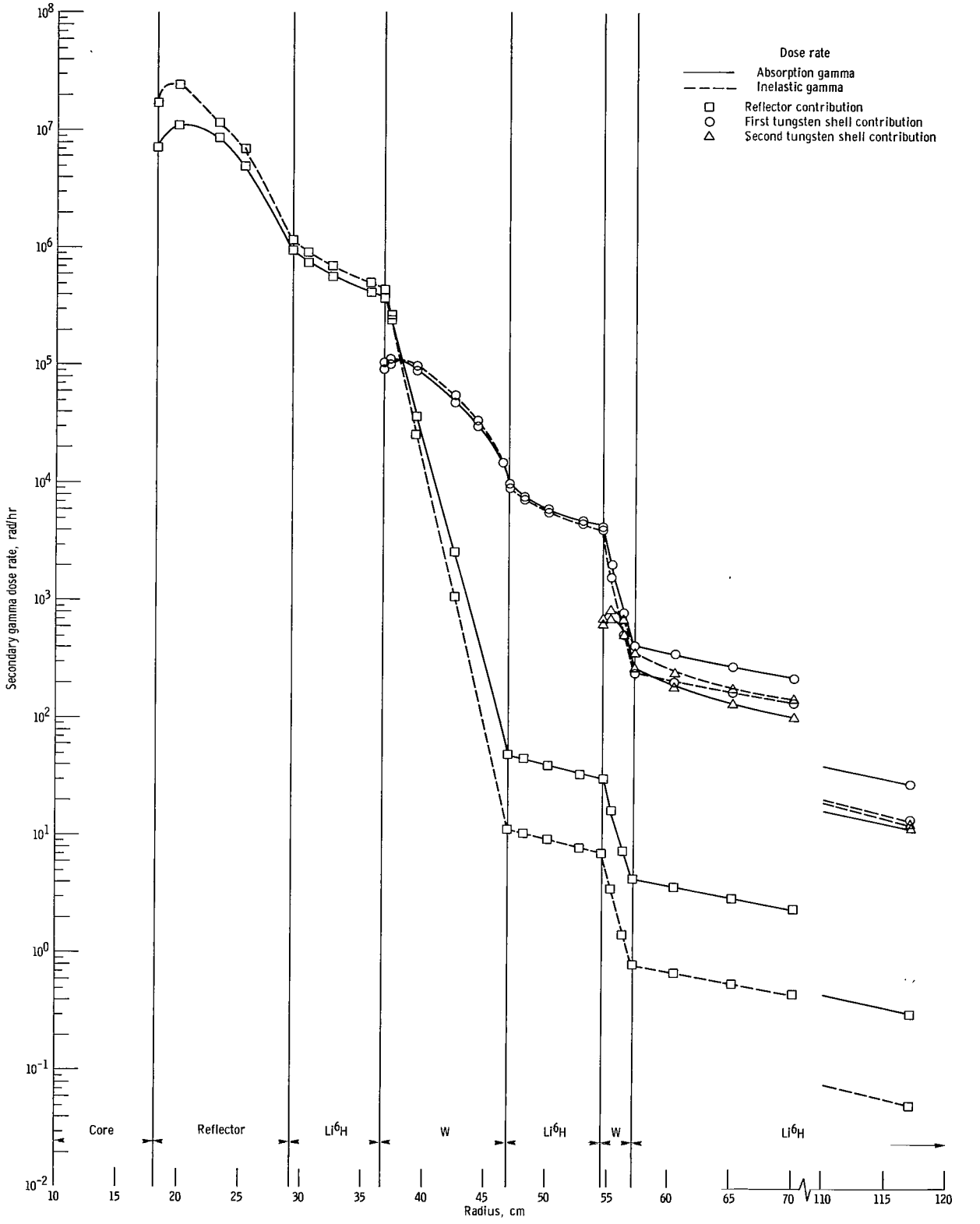

Figure 13. - Secondary gamma dose rates from tungsten reflector and first and second tungsten shields with P_3S_{16} 14-group photon transport calculation for model fast reactor.

in the calculation of the transport of the photons through the laminated shield. The difference could be attributed, in part, to the following:

(1) The P_3 elastic scattering order used in the S_n transport method may not be high enough to accurately calculate the deep attenuation of the secondary photons in the reflector.

(2) For the reflector secondaries, the use of a water buildup factor in the QAD code is questionable.

CONCLUDING REMARKS

A study was made of point neutron and gamma sources in spherical media and a spherical reactor laminated shield using the point kernel (QAD) and discrete ordinates (S_n) methods. The S_n method was limited by the available computer to the following: a scattering order of 3, a quadrature order of 16, and 30 groups. From the neutron point fission source study, the following conclusions may be drawn:

1. Based on the agreement with the Monte Carlo results for natural LiH, an S_n transport calculation of the order P_3S_{16} with 30-neutron groups will yield adequate dose rates for neutron penetrations up to 90 centimeters in LiH and Li^6H.

2. From the study of the point fission source in LiH, it was found that various parameters in the S_n transport calculation affected the computed dose:

   a. Reducing the S_n quadrature order from 16 to 12 or 8 resulted in a calculated dose rate that was lower by 10 and 25 percent, respectively, at an LiH thickness of 117 centimeters.

   b. Lowering the elastic scattering order from P_3 to P_1 resulted in a reduction of the calculated neutron dose rate by a factor of 2.5 at 117 centimeters.

   c. Changing the neutron group structure from 30 to 17 reduced the computed dose rate by a factor of 2 at 117 centimeters.

3. The point kernel code QAD can be made to yield adequate dose rates by giving careful consideration to the neutron removal cross section. The slab removal cross sections for the various elements did not give good results when hydrogenous mixtures of these elements were examined. The distributed neutron removal cross sections that were found to give the best results were Li in LiH (0.1000 cm^2/g) and Li^6 in Li^6H (0.1156 cm^2/g).

From the study of the transmission of photons from a point source through a medium of tungsten, the following conclusions were found:

1. Up to approximately 7 centimeters of tungsten, a photon dose rate computed by a P_3S_{16} 16-group transport calculation agreed with the moments method.

2. At 14 centimeters of tungsten, the transport calculation gave dose rates approxi-

mately 40 percent lower than the moments method.

3. Again at 14 centimeters of tungsten, a P_1S_{16} 16-group transport calculation computed a photon dose rate only one-half that of the moments method.

The study of the neutron penetration from the reactor through the laminated shield showed that the QAD dose rate computation agreed with the P_3S_{16} 30-group transport calculation within 40 percent at a radius of 117 centimeters. This agreement was obtained by using the neutron removal cross-section lithium-6 of 0.1156 square centimeter per gram.

In the analysis of the secondary gamma sources produced in the tungsten layers of the laminated shield, the following conclusions were obtained:

1. The 17 neutron energy group split was adequate for a neutron transport calculation to generate photon secondary source strengths and distributions in all the regions of the shield.

2. A P_1 elastic scattering order neutron transport calculation was sufficient to generate the secondary gamma source strength and distribution in the reflector region.

3. In the last tungsten region, the secondary source strength and distribution computed by a neutron transport calculation using a P_1 elastic scattering order differed considerably from that of the P_3 order.

The total secondary gamma dose rates calculated by the QAD point kernel method agreed to within 10 percent with the S_n transport results. However, the secondary dose calculated by the two methods differed considerably for the reflector. This difference can be attributed, in part, to (1) the elastic scattering order of three used in the S_n calculation being insufficient to accurately calculate deep transport of photons, and (2) the use of a water buildup factor in the QAD line-of-sight code to describe the laminated media of the shield.

Lewis Research Center,
National Aeronautics and Space Administration,
Cleveland, Ohio, August 14, 1968,
129-02-04-14-22.

REFERENCES

1. Fieno, Daniel: Transport Study of the Real and Adjoint Flux for NASA Zero Power Reactor (ZPR-1). NASA TN D-3990, 1967.

2. Malenfant, Richard E.: QAD: A Series of Point-Kernel General-Purpose Shielding Programs. Rep. No. LA-3473, Los Alamos Scientific Lab., Apr. 1967.

3. Joanou, G. D.; and Dudek, J. S.: GAM-II. A B_3 Code for the Calculation of Fast-Neutron Spectra and Associated Multigroup Constants. Rep. No. GA-4265, General Dynamics Corp., Sept. 16, 1963.

4. Joanou, G. D.; Smith, C. V.; and Viewig, H. A.: GATHER-II: An IBM-7090 FORTRAN-II Program for the Computation of Thermal-Neutron Spectra and Associated Multigroup Cross-Sections. Rep. No. GA-4132, General Dynamics Corp., July 8, 1963.

5. Lathrop, K. D.: GAMLEG - A Fortran Code to Produce Multigroup Cross Sections for Photon Transport Calculations. Rep. LA-3267, Los Alamos Scientific Lab., Mar. 11, 1965.

6. Celnik, J.; and Spielberg, D.: Gamma Spectral Data for Shielding and Heating Calculations. Rep. No. UNC-5140, United Nuclear Corp. (NASA CR-54794), Nov. 30, 1965.

7. Goldstein, Herbert: Fundamental Aspects of Reactor Shielding. Additon-Wesley Publ. Co., Inc., 1959.

8. Anon.: Protection Against Neutron Radiation up to 30 Million Electron Volts. Handbook 63, National Bureau of Standards, Nov. 22, 1957, p. 7.

9. Astin, A. V.: Physical Aspects of Irradiation. Handbook 85, National Bureau of Standards, Mar. 31, 1964.

10. Mynatt, F. R.; Greene, N. M.; and Engle, W. W.; Jr.: On the Application Of Discrete-Ordinates Transport Theory to Deep-Penetration Fast-Neutron-Dose Calculations in Water. Trans. Am. Nucl. Soc., vol. 9, no. 2, Nov. 1966, pp. 366-368.

11. Kam, Francis B. D.; and Clark, Francis H. S.: Fission Neutron Attenuation and Gamma-Ray Buildup Factors for Lithium Hydride. Nucl. Appl., vol. 3, no. 7, July 1967, pp. 433-435.

12. Blizard, Everett P.; and Abbott, Lorraine S., eds: Shielding. Vol. III, Part B of Reactor Handbook. Second ed., Interscience Publ., 1962.

13. Lahti, Gerald P: Fission Neutron Attenuation in Lithium 6, Natural Lithium Hydride, and Tungsten. NASA TN D-4684, 1968.

14. Goldstein, Herbert; and Wilkins, J. Ernest, Jr.: Calculations of the Penetrations of Gamma Rays. Rep. NDA-15C-41, Nuclear Development Assoc., Inc. (AEC Rep. NYO-3075), June 30, 1954.

15. Lahti, Gerald P.; Lantz, Edward; and Miller, John V.: Preliminary Considerations for Fast-Spectrum, Liquid-Metal Cooled Nuclear Reactor Program for Space-Power Applications. NASA TN D-4315, 1968.

"The aeronautical and space activities of the United States shall be conducted so as to contribute . . . to the expansion of human knowledge of phenomena in the atmosphere and space. The Administration shall provide for the widest practicable and appropriate dissemination of information concerning its activities and the results thereof."

—NATIONAL AERONAUTICS AND SPACE ACT OF 1958

NASA SCIENTIFIC AND TECHNICAL PUBLICATIONS

TECHNICAL REPORTS: Scientific and technical information considered important, complete, and a lasting contribution to existing knowledge.

TECHNICAL NOTES: Information less broad in scope but nevertheless of importance as a contribution to existing knowledge.

TECHNICAL MEMORANDUMS: Information receiving limited distribution because of preliminary data, security classification, or other reasons.

CONTRACTOR REPORTS: Scientific and technical information generated under a NASA contract or grant and considered an important contribution to existing knowledge.

TECHNICAL TRANSLATIONS: Information published in a foreign language considered to merit NASA distribution in English.

SPECIAL PUBLICATIONS: Information derived from or of value to NASA activities. Publications include conference proceedings, monographs, data compilations, handbooks, sourcebooks, and special bibliographies.

TECHNOLOGY UTILIZATION PUBLICATIONS: Information on technology used by NASA that may be of particular interest in commercial and other non-aerospace applications. Publications include Tech Briefs, Technology Utilization Reports and Notes, and Technology Surveys.

Details on the availability of these publications may be obtained from:

SCIENTIFIC AND TECHNICAL INFORMATION DIVISION

NATIONAL AERONAUTICS AND SPACE ADMINISTRATION

Washington, D.C. 20546